A Generalized Machine Fault Detection Method Using Unified Change Detection

Wenyi Wang, David Forrester and Peter Frith

Aerospace Division, Defence Science and Technology Organisation, Melbourne, VIC 3207, Australia

Wenyi.Wang@dsto.defence.gov.au
David.Forrester@dsto.defence.gov.au
Peter.Frith@dsto.defence.gov.au

ABSTRACT

Many different techniques have been developed for detecting faults in rotating machinery. This is because different fault types typically require different techniques for the effective detection of the fault. However, for many new or unknown fault types, we have found that the existing detection techniques are either incapable or ineffective, and that we therefore need to come up with brand new methods after the fault event. This can significantly constrain the usefulness and effectiveness of Prognostic Health Management (PHM) systems. In this paper we attempt to look at detecting global changes in the synchronously averaged signals as the machine's health status progresses from healthy to faulty, and to define one unified signal processing technique and its associated condition indicators for the detection of changes caused by various types of faults in rotating machinery. The proposed method is conceptually very simple, and its effectiveness is demonstrated using vibration data from machines with several different types of faults. The results have shown that this single unified change detection approach can be very effective in detecting and trending changes caused by many different types of machine faults.

1. INTRODUCTION

Since the advent of some benchmark technologies, namely the envelope technique for bearing diagnosis in early 1970's by Burchill *et al* (1973) and the time synchronous averaging technique for gear diagnosis in mid to late 1970's by Braun (1975) and Stewart (1977), the field of machine diagnostics has had enormous advancement. Over the last four decades, many techniques have been developed for detecting various types of faults in rotating machinery (e.g. Forrester 1996, McFadden 2000, Wang 2001 and techniques discussed in the review papers by Randall 2011 and Lei 2013, etc.). However, it is typically found that different techniques are required for the effective detection of new types of fault. This need to specifically develop new methods whenever a new type of fault arises can significantly constrain the usefulness and effectiveness of PHM systems, especially for new platforms such as the JSF where the PHM capability is designed in during the early stages of development.

In general, for gear tooth related local faults we tend to employ the residual signal after removing the gear mesh harmonics in the spectrum of synchronous signal averages (Stewart 1977, Forrester 1996, Wang 2001). For a localized bearing fault we will most likely look at the resonance demodulation technique (Burchill 1973, Wang and Harrap 1996). For other common faults like rotor unbalance and shaft misalignment we may try to find changes in the low shaft orders such as the first three orders (Forrester 1996, Larder 1999, Vecer *et al* 2005). In cases of spline or pump faults, we will probably focus on the changes at the relatively higher shaft orders or the pump characteristic frequency and its harmonics (Galati 2007, Becker 2007, Hancock 2006). For turbine engine disk cracks, the state-of-the-art technology is to use tip timing data analysis to detect this type of fault (Wang and Muschlitz 2010). There are many other fault types that involve specific detection techniques.

These techniques are widely employed in health and usage monitoring systems (HUMS) for helicopters. Unfortunately, when new or unknown types of faults occur these methods are often either incapable or ineffective to detect the faults. In 2002, planet carrier plate cracking was a new type of fault found in the main rotor transmission of the Blackhawk and Seahawk fleets around the world. Several techniques including those by Blunt and Keller (2006) and by Wang

and Keller (2007) were specifically developed for the fault type after the fault events. Note that this carrier plate has been re-designed by the manufacturer and the plates with the new design are being retrofitted into the fleet. A more recent example is the crash of a Super Puma utility helicopter in the North Sea in 2009 caused by a gear/bearing fault that was not detected by the onboard HUMS (Jarvis and Sleight 2011). The investigation indicated that the most likely root cause was a spall-induced fatigue crack in the 2nd stage planet gear/bearing in the main transmission gearbox of the helicopter, which propagated though the gear/bearing body and led to the disintegration of the gear/bearing, causing the catastrophic failure of the gearbox. The fatal accident led to the loss of sixteen lives.

There have been previous attempts to develop more versatile methods for detecting various types of faults. These include the parametric model-based approach by Wang and Wong (2000) and Wang (2008) in building a linear prediction model for the healthy-state signal and then using this model as an inverse filter to process the future-state signals. The method was proven effective in many cases, especially in the case of multiple gears on the same shaft, but a consistency problem with the selection of model orders can show up when peculiar perturbations exist in the signal. This is probably due to the nature of parametric modeling and lack of constraints in the optimization process. In other words the method lacks robustness. Other studies were carried out by Man *et al* (2012) to use a versatile sinusoidal model for fault diagnosis in a more robust manner, and by Galati *et al* (2008) to use a generalized likelihood ratio algorithm for detecting bearing faults in helicopter transmissions. The work carried out by Lee (2010) was an attempt of detecting a general class of faults using correlation algorithms in a low cost HUMS.

In this paper we attempt to look at detecting global changes in the vibration signals as a machine's health status progresses from healthy to faulty for various different types of faults, and to find one unified signal processing technique and its associated condition indicators for the detection of these changes. The detection of changes due to machine faults often involves comparison of signals from the healthy-state to the faulty-state of the machine. However, a direct comparison in the time domain is often prohibited simply because these signals are in most cases not phase-aligned. Our unified approach deals with the synchronously averaged or re-sampled vibration signals from a rotating component in the machine as it progresses from a healthy state to a faulty state. The healthy-state signal x is employed as a reference, and it is phase shifted by the phase difference from the future-state (healthy- or faulty-state) signals y. The shifted healthy-state signal x_s is then subtracted from future-state signals y to form the change signals. We expect that fault-induced changes will be captured by the change signal. Statistical measures can then be derived from the change signal as condition indicators, and trended over time for fault detection purposes.

The technique is conceptually very simple, and its effectiveness is demonstrated in the paper. Vibration data from machines with several different types of faults are used for the demonstration. The fault types include gear tooth cracks in simple gearboxes; non-uniform gear tooth wear and vane pump failure in turbo-machinery; and nut looseness and planet carrier plate cracking in helicopter transmission systems. The results show that this single unified change detection approach can be very effective in detecting changes caused by many different types of machine faults. We anticipate that further adaptation and validation of this approach may lead us towards a universal method for fault detection in rotating machinery, including faults in gears, bearings, rotors and pumps.

The main driver of developing such a unified approach is to equip existing and future HUMS and PHM systems with the capability of detecting new and unknown types of faults. The implementation of the proposed technique into an existing health monitoring system should be straight-forward.

2. BACKGROUND OF SIGNAL ALIGNMENT

In gear fault diagnosis, we may tend to assume that the synchronously averaged signals are phase aligned if a tachometer signal is employed as a phase reference signal for the rotating components in the gearbox. However, in many cases, the use of a pulsed phase reference signal means that the zero crossing point (phase alignment point) can only be determined to within one sample point, i.e. the rising edge of the pulse occurs somewhere between two sample points. This means the signal averages are only aligned to within one sample point at the original sampling frequency. Note that if the speed reference were a sinusoidal waveform, the zero crossing point can be determined to greater accuracy by the use of interpolation. Additionally, there may be other error sources in the phase reference signal, such as the speed-dependent pulse amplitude, which may cause the misalignment of averaged signals by more than one sample point.

Taking gear tooth cracking as an example fault type, we will start with two actual signals acquired in a gear tooth crack propagation test conducted at the Defence Science and Technology Organisation (DSTO), Australia (Forrester 1996, Vavlitis 1998). This test series will be described in more detail in Section 5.1. Then we will look at some simulated gear mesh signals to see the necessity for accurate signal alignment and some of the problems that can occur when conducting this alignment.

2.1. Example of Gear Mesh Signal Alignment by Direct Signal Shifting

Figure 1 shows two signals of gear mesh vibration, which came from a spur gear at two stages of tooth cracking. The first one is labeled G6b.071 (signal *x*) where the crack was probably just initiated from the stress-riser notch, i.e. there was no visual indication of crack but the post-test fractography analysis showed an equivalent through-crack length of about 0.7mm. The other signal is G6b.110 (signal *y*) where the tooth crack length was around 50 percent of the tooth width (2.75mm by visual inspection from side, about 3.15mm by fractography analysis). Note that the total length of the projected crack path was 5.82mm for this gear. These two signals have very similar amplitude and their phases are not perfectly aligned. We estimated the phase difference by using maximum cross correlation coefficient to the accuracy of one sampling period, and found that the phase difference corresponds to about 3 sample points. This near-integer-sample phase shift is likely to be due to the on-line angular data acquisition of the G6 test data triggered by the TTL pulses (0-5 volts square pulse, 1024 pulses/rev) of an optical shaft encoder, where each averaged signal might have started from a slightly different TTL pulse. However, this phase shift (i.e. the number of samples) may be different from signal to signal.

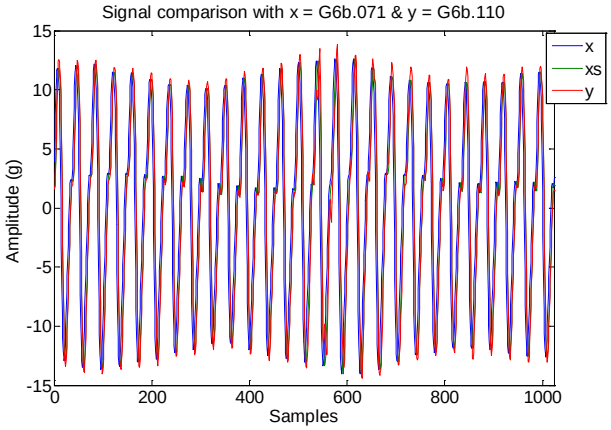

Figure 1. Comparison of synchronous signal averages of gear mesh vibration

The signal *x* is then shifted by 3 samples and the shifted version is denoted by x_s. As we can see in Figure 2, x_s is well aligned with signal *y*. A straight subtraction of x_s from *y* then produces the so-called change signal δ, as shown in Figure 3. Obviously, the change signal has picked up the changes caused by the tooth cracking. It has a kurtosis, as defined in Eq. (12) of this paper, value of 9.3 where a kurtosis value of 3.5 would typically be regarded as an indication of an early localized fault. This is comparable to some of the benchmark indicators, such as a kurtosis of 5.2 for the residual signal, derived by removing the gear mesh harmonics in the spectrum of the Synchronous Signal Average (SSA), or a kurtosis of 11.4 by further removing the 1st and 2nd sidebands of the harmonics. The residual signal kurtosis is one of most commonly used Condition Indicators (CIs) in gear fault diagnosis.

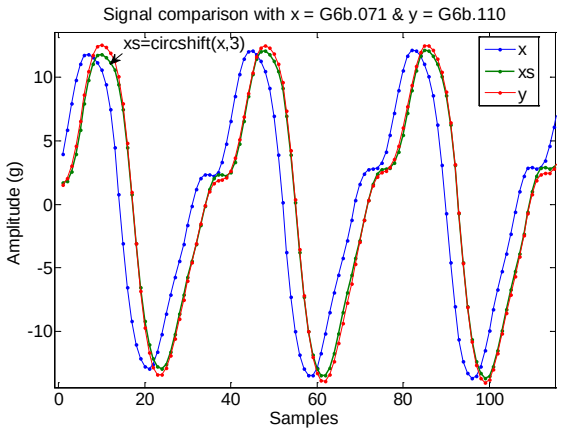

Figure 2. Zoomed version of Fig. 1

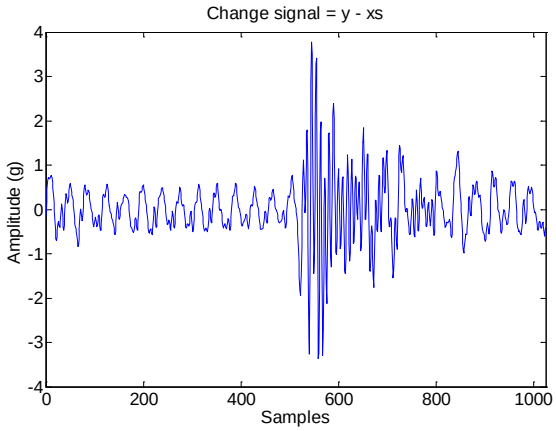

Figure 3. The change signal (full bandwidth): $\delta = y - x_s$, with a kurtosis of 9.3.

Normally, a localized fault tends to cause more changes in relatively high frequency range whereas a distributed fault is more likely to produce changes in low frequency. Therefore, if we view the change signal in two frequency bands, i.e. a low-order band and a high-order band, where the cross-over occurs at 85 shaft orders (which is just above the 3rd gear mesh harmonic at 3×27 = 81 orders and is below a structural resonance), as shown in Figure 4, we can see that the crack-induced change in the high-order band is far more pronounced than that in the low-order band. The kurtosis values for these two bands are 16.5 and 3.8 respectively.

Intuitively, we can say that the key step here is to align signals acquired in a healthy-state (or reference signal) and a faulty-state (or monitored signal). We can also use the instantaneous phase cross correlation to obtain sharper maxima so that the signal shift amount may be defined more clearly. However, to achieve signal alignment with an

accuracy better than one sample period, we will need to interpolate the cross correlation function.

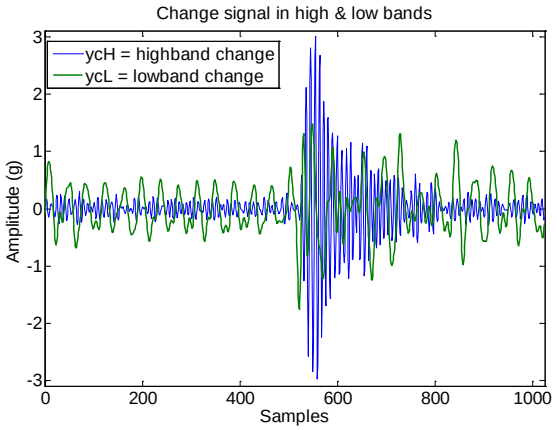

Figure 4. The change signal divided into high- and low-order bands, with the kurtosis values of 16.5 and 3.8 respectively.

2.2. Understanding Signal Alignment using Simulated Signals

We can see, from the above example, that phase alignment of the two signals is essential. Even in cases where signal averaging has been performed using a phase reference signal from the shaft of interest, small variations in signal alignment from one run to the next may occur. This can be caused by a change in the shaft reference probe (e.g. dirt, physical movement of the sensor, etc.), and, more likely, the inherent errors in the tachometer signal processing (e.g. errors from interpolating the position of the zero-crossing between sample points). Also, in cases where the phase reference signal sensor is not physically attached to the shaft of interest, or where the synchronous averaging is carried out using a phase reference directly derived from the vibration signal (Bonnardot *et al* 2005), it is not feasible to phase-align the averaged signals during the synchronous averaging process.

For the remaining part of the paper, we denote a uniform phase shift by $\Delta\theta$ and a uniform time delay by Δt as shown in the following expression. The word 'uniform' applies to multi-frequency signatures, where the phase shift and time delay are the same for all the frequency components.

$$y(t) = \sum_k A_k \cdot \sin\left[2\pi\ f_k(t-\Delta t) + (\theta_k + \Delta\theta)\right]$$

2.2.1. Uniform phase shift

First of all, when talking about phase alignment we may tend to think of aligning the initial phase of the signal. If we have a test signal of

$$x(t) = \sin(2\pi \cdot 27 \cdot t + 0.987)$$

with a sampling rate of 1024 samples/second, i.e. $t = (0{:}1023)/1024$, and an arbitrary initial phase of $\theta = 0.987$ radians, and we then define a phase-shifted version of this signal, $y(t)$, where the initial phase of this frequency component is changed by $\Delta\theta = -0.4975$ radians from $x(t)$, then this phase shift will correspond to almost exactly 3 sample points, i.e. $1024\times0.4975/(2\pi\times27)=3.003$. Therefore, to align $x(t)$ and $y(t)$ we could simply shift signal $x(t)$ by 3 sample points, e.g. using the Matlab function '*circshift*': x_s = circshift(x,3). However, if the phase shift does not correspond to a near-integer sample point, then this alignment process will not work. Figure 5 shows the signal $y(t)$ with a phase shift of –0.57 radians (or 3.4406 samples) and the signal $x(t)$ shifted by 3 sample points. As can be seen, rounding to the nearest sample point does not produce a good result, and a finer (fractional-point) shift resolution is required.

Now let us employ a two-component sinusoid like

$$x(t) = \sin(2\pi \cdot 27 \cdot t + 0.987) + \sin(2\pi \cdot 2 \cdot 27 \cdot t + 1.053)$$

where the 2nd component is a harmonic of the 1st one. Signal $y(t)$ is then defined as signal $x(t)$ shifted by –0.4975 radians at both frequency components (i.e. uniform phase shift). If we now shift $x(t)$ by 3 sample points using '*circshift*' we cannot get a good alignment as shown in Figure 6. This is because the phase shift of –0.4975 radians for the higher frequency component corresponds to almost 1.5 sample points instead of 3 for the lower frequency component, i.e. $1024\times0.4975/(2\pi\times2\times27) = 1.5015$.

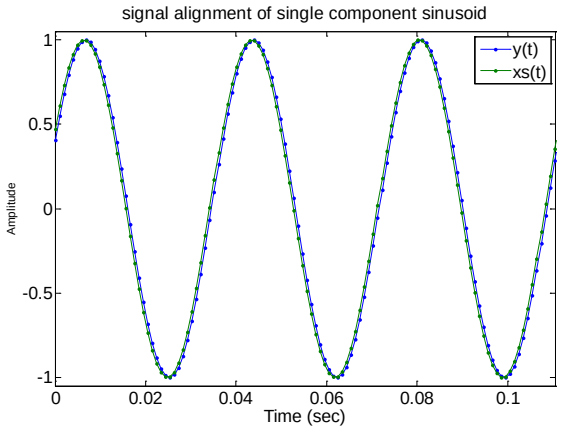

Figure 5. Simulated signal x_s & y showing that direct signal shifting would not work with a phase shift of non-integer sample.

There are two important observations from this section: (1) direct signal shifting by integer sample points would not be a good approach if the phase difference does not give a time delay corresponding to integer number of data samples; (2) direct signal shifting is also no good for multiple components signals where the phase shift is the same across all the frequency components.

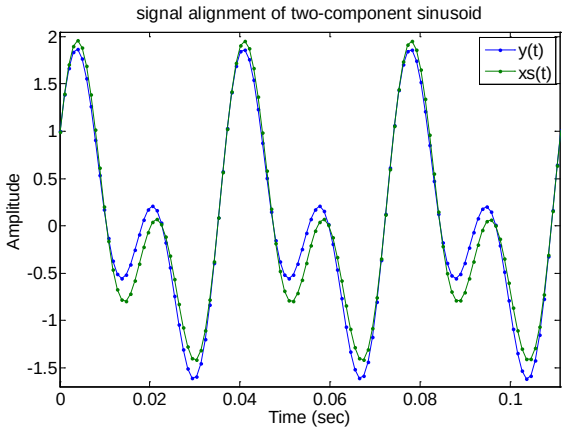

Figure 6. Simulated signal x_s & y showing that direct signal shifting would not work with uniform phase shift in multi-component sinusoid signal

2.2.2. Uniform time delay

For the process of synchronous signal averaging, any errors and/or differences in the phase reference signal and zero-crossing point will consequently produce a uniform time delay across all frequency components in the averaged signal. This is the underlying cause of phase misalignment between SSAs.

For the above example with

$$x(t) = \sin(2\pi \cdot 27 \cdot t + 0.987) + \sin(2\pi \cdot 2 \cdot 27 \cdot t + 1.053)$$

and

$$y(t) = x(t - 0.0205),$$

the time delay of 0.0205 seconds corresponds to almost 21 samples (i.e. 0.0205×1024 = 20.992), so direct signal shifting should work fine. However, direct signal shifting will not work when the uniform time delay is 0.02 seconds, as this corresponds to 20.48 samples. It would not be hard to imagine what difference this nearly half-a-sample shifting error is going to make in the change signal. This is a very likely scenario with synchronous signal averages because any differences between the phase reference signals from one signal average to the next are almost certainly going to occur in non-integer samples – although some can be really close to integers, such as the gear signals shown in section 2.1 where an optical shaft encoder was used.

An alternative approach to direct signal shifting in the time domain is to carry out the shift in the frequency domain. Figure 7 shows an example of aligning two signals involving a uniform time delay of 0.02 second (or 20.48 samples) by shifting the phase spectrum of x and then transforming back to the time domain. The theory behind this example will be given in the next section. We can see in Figure 7 that the shifted x (x_s) is perfectly aligned with signal y. In fact, this approach applies to both cases of uniform phase shift and uniform time delay.

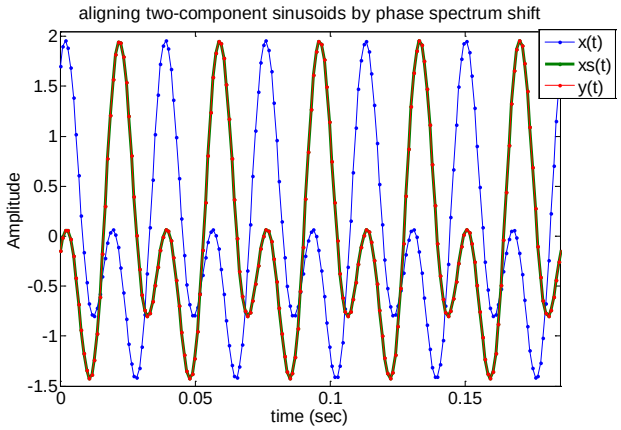

Figure 7. Alignment of signals with a 0.02 second time delay (at 1024 sampling rate) via shifting the phase spectrum of x by the difference between phase spectra of x and y

3. THEORETICAL DEVELOPMENT OF UNIFIED CHANGE DETECTION APPROACH

From the last section, we have shown that the future-state signal $y(t)$ can be aligned with the healthy-state signal $x(t)$ by introducing a time shift. In other words, alignment of the signals means a simple time shift by $-\Delta t$ which is the lag that gives the maximum value of the cross-correlation function. It can be carried out in the frequency domain. Mathematically, if we assume that signal $y(t)$ is a time shifted version of signal $x(t)$, and ignore the amplitude difference, we have

$$y(t) = x(t - \Delta t) \tag{1}$$

Taking the Fourier transform on both sides of Eq. (1) and making use of the translation property of Fourier transform, we get

$$\begin{aligned} Y(f) &= X(f)e^{-j2\pi \Delta t f} \\ A_Y(f)e^{j\Phi_Y(f)} &= A_X(f)e^{j\Phi_X(f)}e^{-j2\pi \Delta t f} \\ A_Y(f)e^{j\Phi_Y(f)} &= A_X(f)e^{j[\Phi_X(f) - 2\pi \Delta t f]} \end{aligned} \tag{2}$$

where the amplitude and phase spectra are given by

$$\begin{aligned} A_X(f) &= |X(f)|, \quad \Phi_X(f) = \angle X(f) \\ A_Y(f) &= |Y(f)|, \quad \Phi_Y(f) = \angle Y(f) \end{aligned} \tag{3}$$

By ignoring the amplitude difference, or making $A_Y(f) = A_x(f)$, we have

$$\begin{aligned}\Phi_Y(f) &= \Phi_X(f) - 2\pi\,\Delta t\, f \\ 2\pi\,\Delta t\, f &= \Phi_X(f) - \Phi_Y(f)\end{aligned} \tag{4}$$

From Eqs. (2) and (4), we can see that time-shifting $x(t)$ by Δt , i.e. $x(t-\Delta t)$ is equivalent to shifting the phase spectrum of $x(t)$ by the difference of phase spectra of $x(t)$ and $y(t)$. The time-shifted $x(t)$ will be aligned with $y(t)$. Hence we don't really need to know the lag Δt via cross-correlation and interpolation.

Now, we put the amplitude difference back, the Fourier transforms of signal $x(t)$ and $y(t)$ are respectively given by

$$\begin{aligned}X(f) &= \int_{-\infty}^{\infty} x(t)\cdot e^{-j2\pi f t}\mathrm{d}t = A_X(f)\cdot e^{j\Phi_X(f)} \\ Y(f) &= \int_{-\infty}^{\infty} y(t)\cdot e^{-j2\pi f t}\mathrm{d}t = A_Y(f)\cdot e^{j\Phi_Y(f)}\end{aligned} \tag{5}$$

The difference of phase spectra is

$$\Delta\Phi_{XY}(f) = \Phi_X(f) - \Phi_Y(f) \tag{6}$$

Shifting the phase spectrum $X(f)$ by the difference given in Eq. (6), which is equivalent to time-shifting $x(t)$ by Δt , i.e. $x(t-\Delta t)$, we have the Fourier transform of the shifted signal

$$\begin{aligned}\hat{X}(f) &= A_X(f)e^{j[\Phi_X(f)-2\pi\Delta t f]} \\ &= A_X(f)\cdot e^{j\cdot[\Phi_X(f)-\Delta\Phi_{XY}(f)]} \\ &= A_X(f)\cdot e^{j\cdot[\Phi_X(f)-(\Phi_X(f)-\Phi_Y(f))]} \\ &= A_X(f)\cdot e^{j\cdot\Phi_Y(f)}\end{aligned} \tag{7}$$

We can derive the shifted version of signal $x(t)$ by an inverse Fourier transform

$$\hat{x}(t) = \int_{-\infty}^{\infty} \hat{X}(f)\cdot e^{j2\pi f t}\mathrm{d}f \tag{8}$$

which is a real-valued signal as $x(t)$ and $y(t)$ are both real-valued so that $A_X(f)$ is even and $\Phi_Y(f)$ is odd.

Having had $x(t)$ and $y(t)$ aligned, we can now define the change signal as

$$\delta_{xy}(t) = y(t) - \hat{x}(t) \tag{9}$$

On the other hand, we will see that the Fourier transform of the change signal is

$$\begin{aligned}\Delta_{XY}(f) &= Y(f) - \hat{X}(f) \\ &= A_Y(f)\cdot e^{j\cdot\Phi_Y(f)} - A_X(f)\cdot e^{j\cdot\Phi_Y(f)} \\ &= \left[A_Y(f) - A_X(f)\right]\cdot e^{j\cdot\Phi_Y(f)}\end{aligned} \tag{10}$$

Therefore, we can also define the change in the spectral domain. Notice that the amplitude in Eq. (10), $[A_Y(f)-A_X(f)]$, may be negative at some frequencies, which means a phase shift of π to those frequency components. The change signal in the time domain is then obtained by an inverse Fourier transform

$$\delta_{xy}(t) = \int_{-\infty}^{\infty} \Delta_{XY}(f)\cdot e^{j2\pi f t}\mathrm{d}f \tag{11}$$

For reasons mentioned in the first example in Section 2.1, it is often necessary to select a cross-over frequency in shaft orders to divide the change signal into high & low bands when changes are not obvious in the full-band. Therefore, for fault detection and trending purposes the change signal can be viewed from three perspectives, i.e. in low-band, high-band and full-band.

4. DERIVATION OF CONDITION INDICATORS

Three condition indicators (CIs) are defined in this section. These CIs can be used as measures of the machine health state; they can be trended over time for fault detection purposes. In Section 5, the unified change detection technique with these CIs is applied to the detection of several different types of faults.

4.1. Kurtosis of the change signal

Kurtosis is the 4th order statistical moment normalized by the standard deviation to the 4th power; it is often used as the CI for localized gear and bearing faults, such as gear tooth cracking and bearing element spalling. These local faults cause spikiness in fault signatures and kurtosis is an effective indicator for spikiness in the signal. For a discrete change signal $\delta(n)$, n = 1, 2, … N, with a mean value of $\bar{\delta}$, the kurtosis is defined as

$$K_\delta = \frac{N\left[\sum_{n=1}^{N}\left(\delta(n)-\bar{\delta}\right)^4\right]}{\left[\sum_{n=1}^{N}\left(\delta(n)-\bar{\delta}\right)^2\right]^2} \tag{12}$$

If the change signal is Gaussian noise, the above kurtosis will be around 3. In gear fault diagnosis, many healthy-state residual signals (after removing gear mesh harmonics and their sidebands) are sub-Gaussian with kurtosis values slightly less than 3. Kurtosis values of 3.5 and 4.5 are generally regarded as the alert and alarming levels respectively. Usually, the high-band kurtosis is more sensitive to sharp spikes induced by localized faults. However, kurtosis may not necessarily be good when it is used as a trending parameter because spikiness can be reduced in the change signal as localized fault develops into distributed fault, especially in cases of bearing faults.

4.2. Energy ratio of the change signal

The standard deviation or root mean square (RMS) value of the change signal can also be employed as a trending parameter to continuously monitor the condition changes in rotating machinery. We define energy ratio as the ratio between the RMS of the change signal and the RMS of the healthy-state or reference signal, i.e.

$$E_{\delta,x} = \frac{\sqrt{\sum_{n=1}^{N}\left(\delta(n)-\bar{\delta}\right)^2}}{\sqrt{\sum_{n=1}^{N}\left(x(n)-\bar{x}\right)^2}} \tag{13}$$

The energy ratio is used to normalize the energy in the change signal against the constant energy in the reference signal. Ideally, we can expect the energy ratio to increase as the fault progresses from early to late stages provided that the fault-induced changes are well reflected in the change signal. However, the randomness in the CI may not make the increasing trend strictly monotonic.

4.3. Scaled Kurtosis of the change signal

We define the scaled kurtosis as the product of the kurtosis of the change signal and the energy ratio given by Eqs. (12) & (13). Mathematically, the expression for scaled kurtosis is

$$\begin{aligned}\hat{K}_{\delta,x} &= K_{\delta}\cdot E_{\delta,x} \\ &= \frac{N\left[\sum_{n=1}^{N}\left(\delta(n)-\bar{\delta}\right)^4\right]}{\left[\sum_{n=1}^{N}\left(\delta(n)-\bar{\delta}\right)^2\right]^{3/2}\cdot\left[\sum_{n=1}^{N}\left(x(n)-\bar{x}\right)^2\right]^{1/2}}\end{aligned} \tag{14}$$

It combines the change signal with the reference signal, so that the condition is always compared to a common reference. As we can see in the following applications, this CI can give a more consistent trending of fault conditions than the kurtosis itself. A reasonable explanation for the results would be that, in the early stages of fault development (when the fault is localized), the kurtosis performs more effectively than the energy ratio. However, in late stages of fault development (when the fault may be more distributed), the spikiness in the change signal drops but the energy level in the change signal increases rapidly, which will lead to an overall increase in the scaled kurtosis (the product).

5. APPLICATIONS OF THE UNIFIED CHANGE DETECTION APPROACH

We have defined the approach to deriving the change signals from the healthy-state signal to the future-state signals. With the change signals, we have proposed three condition indicators in three frequency bands. This will produce nine CIs for each future-state signal. Trending these CIs over time will allow changes in the condition of the monitored component of the machine to be detected. In this section, we will demonstrate the effectiveness and robustness of the proposed method in a number of different fault cases involving different fault types.

Vibration data from machines with several types of faults are used for the demonstration. The fault types include gear tooth cracks in a simple gearbox; non-uniform gear tooth wear and vane pump failure in turbo-machinery; and nut looseness and planet carrier plate cracking in helicopter transmission systems. Using the same unified approach, we have produced various trending curves for each of these fault types. The results have shown that this single unified change detection approach can be very powerful in detecting changes caused by many different types of machine faults. In practice all nine CIs should be trended during machine operations. As there is not enough space in this paper to show results for all nine CIs, we will show results for some selected CIs in the following examples.

5.1. Application to Detecting Gear Tooth Crack Growth

The study of tooth crack development and propagation in the pinion spur gear of a test gearbox were performed by Swinburne University of Technology and DSTO (Forrester 1996, Vavlitis 1998). The test gearbox was a simple single-stage reduction gearbox with 27 teeth on the driving pinion and 49 teeth on the driven gear (i.e. the gear ratio was r = 27/49). The gearbox was driven by an electric motor through a belt drive. The load to the test gear was provided by a dynamometer with a full loading capacity of 45kW at 40Hz input shaft speed. The test gears, labeled G6, A1, A2, A3 and A5 etc, were the input pinion (with a rated load of 27.5kW) with a semi-circular spark-eroded notch (2mm×0.1mm×1mm) at the root fillet in the middle of the tooth width. The notch was designed as a stress riser for crack initiation during the test. The gear was made of EN36A case hardening low alloy steel with teeth precision-ground under AGMA Class 13 standard. The input speed of the gearbox was set to a nominal value of 2400rpm (40Hz), which was varied during the test in a range of 38.6 to 39.3Hz. Results with selected CIs for G6, A3 & A5 are shown here.

Figure 8 shows the trending curve for G6 scaled kurtosis in the high band (cross-over at 85th shaft order) from files G6b.071 to G6b.110, the dataset used here is the same as that used in Section 2.1. We can see that the scaled kurtosis CI generally trends upwards with the increasing crack size. However, the general trend was disrupted at file #97. This was caused by the inspection after file #96, where the faulty gear was dismantled from the test rig and the tooth crack was forced to open with a static overload for magnetic rubber inspection of crack size. It is believed that the inspection process interrupted the crack progression, i.e. the static overload caused crack retardation or arrest. Figure 9

shows the trending curves of energy ratio CIs in full, high and low order bands. Obviously, the high band (blue line) is most sensitive to the changes caused the increasing crack size.

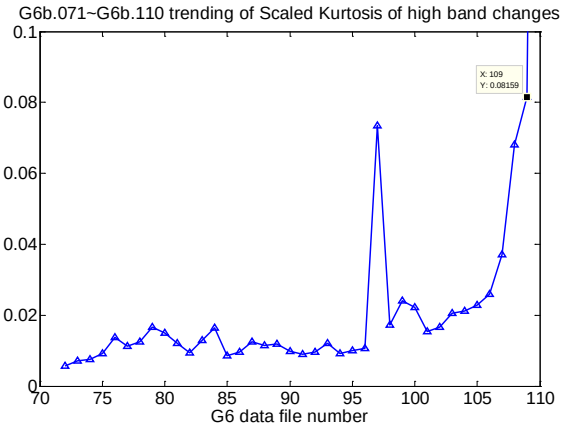

Figure 8. Trending of G6 scaled kurtosis in high-band from G6b.071 to G6b.110 (the value at G6b.110 was 0.66 – outside the displayed range).

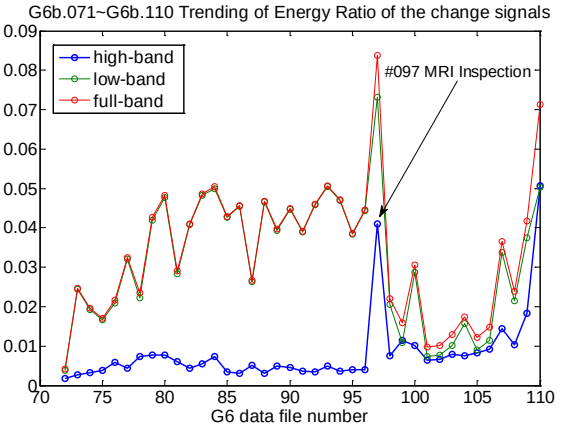

Figure 9. Trending of G6 energy ratio in all three bands for (G6b.071~110) under 45kW load, crack growth disrupted by an inspection.

While the results shown in Figure 8 and Figure 9 are possibly affected by interrupted tooth crack growth, Figure 10 shows the trending curve of high band kurtosis for an uninterrupted growth from G6b.149 to G6b.155. The reference signal was G6b.148 where the tooth crack size was estimated to be 3.63mm by post-test fractography analysis. By G6b.155 (the last data file for the G6 test), the tooth crack grew to an advanced stage where the cracked tooth was just about to fall off, and the crack length was measured at 4.67mm by fractography analysis (80 percent tooth body cracked, as compared to the crack path length of 5.82mm). Note that the kurtosis values in this plot do not represent the change between the faulty-state and healthy-state, rather the change was from a 'less faulty' to 'more faulty' state (i.e. the normal alert and alarm levels of 3.5 and 4.5 do not apply here). Figure 11 shows the change signals from G6b.148 to G6b.155 in the high and low bands.

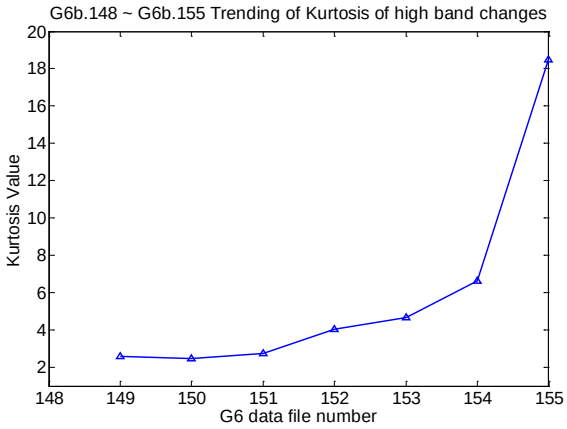

Figure 10. Trending of G6 kurtosis in high-band for G6b.148~155, a further uninterrupted crack growth under constant load (24.5kW) after G6b.110.

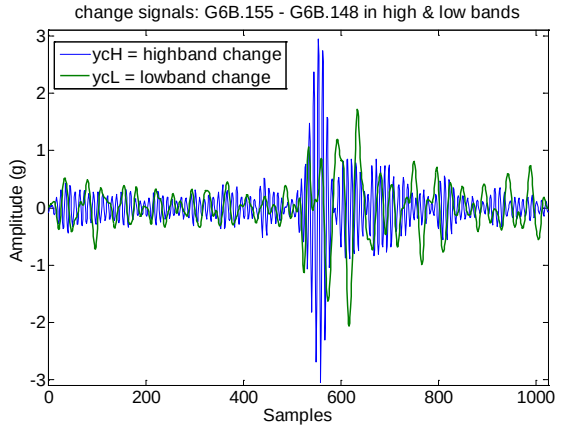

Figure 11. Change signal from G6b.148 to G6b.155.

More results are given in Figure 12 and Figure 13 for the DSTO gear tooth crack propagation test series using the identical type of test gears. Figure 12 shows the A3 gear test trending curve of scaled kurtosis from A3B2.501 to A3B2.549 over some 27.5 minutes of testing (about 66000 fatigue cycles to the cracked tooth with constant load of 30kW at 40Hz shaft speed). In this test period, the crack had uninterrupted continuous growth from 4.89mm to 5.84mm along a curved crack path (Vavlitis 1998, where A3 was labelled as A2-3). With file A3B2.549, the kurtosis of the change signal in high order band is 9.49, as compared to the conventional residual kurtosis of 5.09.

Similarly, Figure 13 shows the A5 gear test trending curve of scaled kurtosis from A5B0.598 to A5B0.763 over some 84 minutes of testing (about 201600 fatigue cycles to the cracked tooth with 40Hz shaft speed) where the crack had uninterrupted continuous growth from 1.46mm to 2.27mm along a curved crack path (Vavlitis 1998, where A5 was

labelled as A2-5). With file A5B0.763, the kurtosis of the change signal in the high order band is 9.0, as compared to the conventional residual kurtosis of 4.3. If we pay close attention to the values on the vertical coordinate (scaled-kurtosis) in Figure 12 and Figure 13, we could find that these values might be a reflection of the crack sizes, e.g. the scaled kurtosis value of 0.44 for A3B2.549 with a crack length of 5.84mm versus the scaled kurtosis value of 0.174 for A5B0.763 with a crack length of 2.27mm. However, this could also be affected by the load.

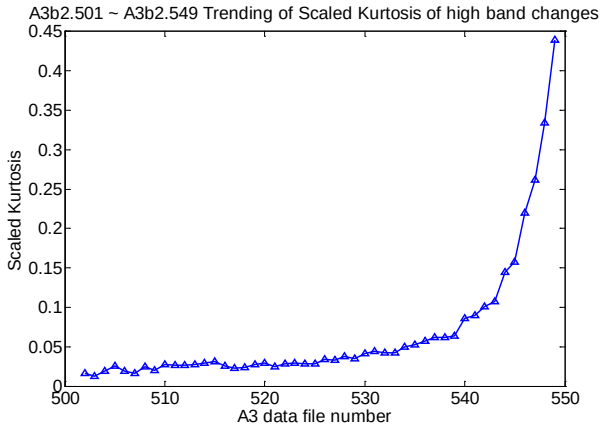

Figure 12. CI trending of A3B2.501~549 data – final crack size 5.84mm with uninterrupted crack growth under 30kW load.

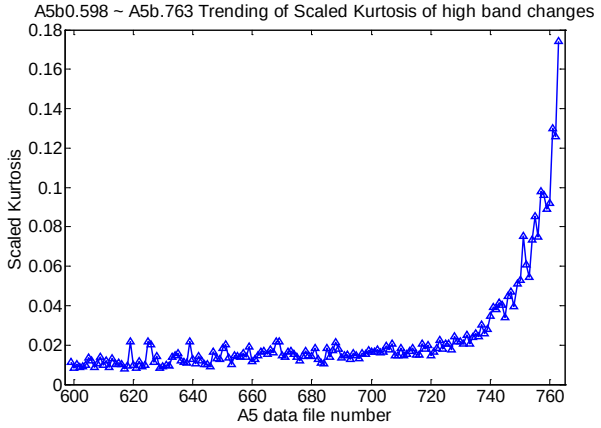

Figure 13. CI trending of A5B0.598~763 data – final crack size 2.27mm with continuous progression without interruption under constant load of 45kW.

We have also conducted a more detailed comparison study between the unified change detection approach and other commonly used gear fault detection techniques. Figure 14 shows the results of comparing the unified approach with two other methods based on the autoregressive (AR) model residual and the conventional residual signals using the A3 gear test data. We find that the changes picked up by the unified approach increase more rapidly than the other two methods, and the AR model result is very much dependent on the selection of model order, and whether the AR model is built on a reference signal or the monitored signal itself. The unified approach has shown more fluctuation in the result, which could be smoothed out by using the scaled kurtosis as shown in Figure 12.

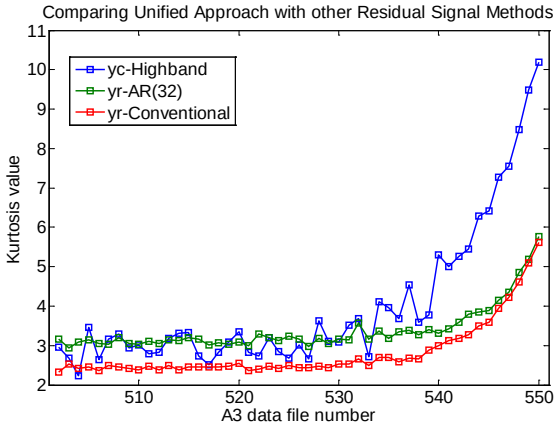

Figure 14. Comparative study between unified change detection approach and other methods based on self-AR(32) residual and conventional residual signals using the DSTO A3 gear tooth cracking data

We can draw some conclusions based on the results of the comparison study using the DSTO gear rig data. The unified approach: (1) requires less prior knowledge, it only needs to choose the high & low band cross-over frequency (e.g. at the lower bound of a resonance or the upper bound of the significant gear mesh harmonics); (2) is much more versatile than conventional residual signal method in which we must know which orders to be removed; (3) is capable of dealing with cases of multiple gears on the same shaft and is more robust than the AR residual method where a consistent model order selection is lacking; and (4) gives better and more robust trending capability by using a scaled kurtosis CI than a conventional kurtosis CI.

5.2. Application to Detecting Faults in Turbomachinery

We have found in the last section that the unified change detection approach is effective in detecting localized changes induced by gear tooth cracking, especially by using a high band CI. In this section, we will find if this approach can be employed for the detection of distributed faults such as uneven wear on many teeth of a gear, and damage to all the vanes of a vane pump. The results show that low-band and full-band CIs are very sensitive to the changes caused by these distributed faults.

5.2.1. Non-uniform Gear Tooth Wear

In gear design, it is normal practice to select the number of teeth for a gear pair such that there is no common factor between them. This allows each tooth of one gear to mesh with every tooth of the other gear, and therefore promotes

even wear of the teeth. This system is usually referred to as the hunting tooth system. In the gearbox of a developmental turbofan, there was a non-hunting tooth system with a common factor of 3 between the tooth counts, which resulted in damage (non localized uneven wear) to every 3rd tooth on the pinion. Now, we employ the unified change detection approach to monitor the changes induced by this specific wear pattern over time.

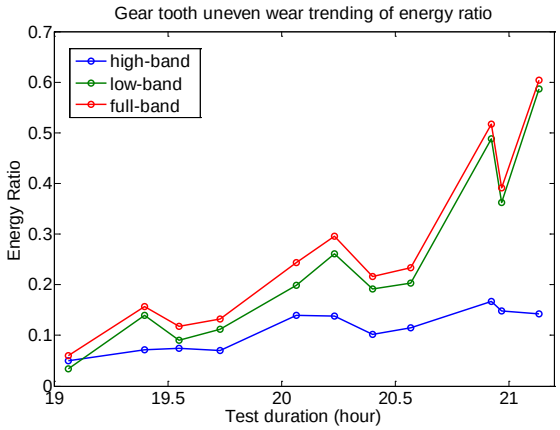

Figure 15. Turbo-fan gear CI (energy ratio) trending with Channel 3 data and cross-over frequency of 5 shaft orders.

The reference signal *x* was acquired at about 19 hours of testing, and 12 monitoring signals (*y*) were acquired after signal *x*. Figure 15 shows the trending curve of the energy ratio CI in full, low and high order bands versus the accelerated test time over a period of more than 2 hours. The increasing trend of the full (red line) and low (green) band CIs clearly shows the progression of the uneven wear to every 3rd tooth on the pinion gear. The high (blue) band CI has a less obvious trend. These results were obtained with a cross-over frequency of 5 shaft orders; so it means that most of the energy in the change signal is in the low band below the 5th shaft order. In fact, the high band CI is of little importance in this case as the distributed fault would not necessarily bring any high frequency resonance features.

5.2.2. Vane Pump Failure

This fault type is about the severe damage to all the vanes in a vane pump attached to the accessory gearbox of an aircraft engine. The vibration data were recorded at three stages of an accelerated test when the engine was running on full power. They were from *a*) early stage – within the first 10 percent of the testing time; *b*) late stage – between 80 ~ 90 percent of the testing time and *c*) last stage – within the last 2 percent of the testing time of the accelerated test. Altogether, there were 36 tri-axial vibration data files used for producing the results shown in this paper, where the first one in the early stage was used as the reference.

Figure 16 shows the trending curves of scaled kurtosis CI in three bands using the horizontal axial (the most sensitive direction) vibration data. Along the abscissa coordinate of the plot there are 35 columns of CI points; the first 11 files were from the early stage of testing, the following 18 files were from the late stage and the last 6 files from the last stage of testing. The cross-over frequency for the low and high bands was selected at just above the 6th harmonic of the vane pass frequency. We can see in Figure 16 that the full band (red) and low band (green) CIs show prominent step changes across the three stages of testing. The high band (blue) CIs show some indication of change but this is not as prominent as the other two bands. This is because the signal changes caused by the vane damage are mostly likely located at the vane pass frequency and its lower harmonics. Obviously, the changes detected by the unified approach can give sufficient lead time to the failure of the vane pump. The pump actually failed on the very next run after the last data file was recorded.

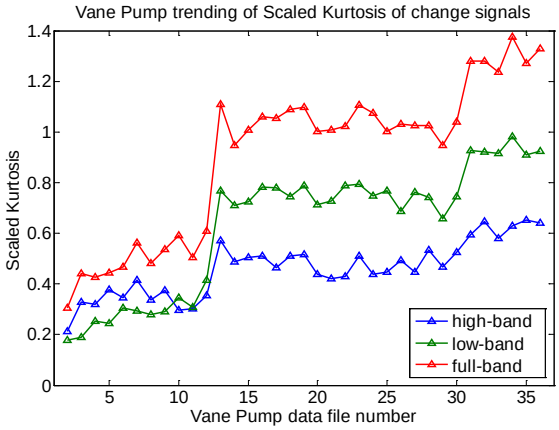

Figure 16. Aero-engine vane pump CI (scaled-kurtosis) trending with Channel 3 data and cross-over frequency of 65 shaft orders.

5.3. Applications to Detecting Faults in Helicopter Transmission Systems

Health and Usage Monitoring Systems (HUMS) have been used in helicopter transmission gearboxes for many years. In general, existing HUMS can detect faults of common types such as gear and bearing faults without great difficulty. However, less common or unknown types of faults are difficult to detect. In this section, we will present two cases of less common fault types and employ the proposed unified approach to trend the progression of these faults.

5.3.1. Input Shaft End Nut Looseness

The first of these less common fault types is the end nut looseness at the bevel input pinion extension shaft in a helicopter Main Rotor Gearbox (MRG). This is a fault type which is believed to be the most likely cause of the rupture

of the extension shaft. It can be induced by a lack of tightening torque of the end-nut and consequently causes a load redistribution in the MRG assembly. A study was conducted at DSTO into this fault type using a light utility helicopter MRG in DSTO's Helicopter Transmission Test Facility (HTTF). The objective of the study was to provide HUMS systems with the capability to detect the loss of tightening torque of the end-nut and to prevent the rupture of the input pinion extension shaft.

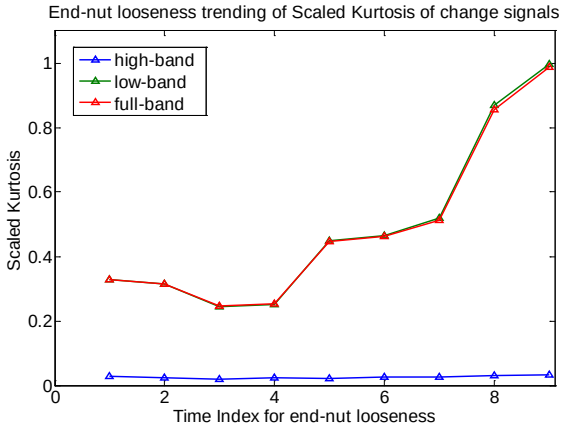

Figure 17. Trending of scaled kurtosis CI from pinion SSA (at Ring-Front sensor & cruise power) change signal with cross-over at 75th shaft order

Ten end-nut tightening torques were used in the test, i.e., 100 percent, 91%, 78%, 67%, 56%, 44%, 33%, 22%, 11% and 7% of the nominal tightening torque. The data recorded at 100% tightening torque were used as the reference, and the tightening torque is assumed to become less and less over time. The 7 percent torque (a very loose condition) was found to be the thread breaking torque at which we could just start to turn the end-nut. Throughout the test, the input shaft speed was kept at the nominal level (about 100Hz) and there was no mast load applied to the MRG. The data used in this paper were acquired under the forward flight condition at 75 percent maximum power.

Using the synchronous signal averages (SSA) with respect to the input pinion shaft and the planet carrier shaft, we produced the scaled-kurtosis CIs at each level of the tightening torque and plotted them in Figure 17 and Figure 18. The abscissa coordinates in the plots can be considered a time progression index where each point corresponds to the next looser level of the tightening torque, i.e. time index 1 corresponds to the 91%, index 2 is 78% … and index 9 is 7% tightening torque.

From Figure 17 which is based on the input pinion SSA change signals, we can see that the end-nut loosening condition can be detected by the full (red) and low band (green) CIs from time index #5 (i.e. 44% tightening torque), and becomes very obvious at index #8 (or 11% tightening torque). On the other hand, Figure 18 shows the CI trending based on the planet carrier SSA change signals. Here, it could be argued that the end-nut loosening condition is detectable by the full (red) and high band (blue) CIs from time index #3 (i.e. 67% tightening torque) forward, which is apparently better than the result in Figure 17. This result may be because the effect of load redistribution caused by the loosening end-nut on the input shaft was magnified at the carrier shaft by the reduced speed and increased torque. The results have shown that the unified approach can be effective in detecting faults of this particular type.

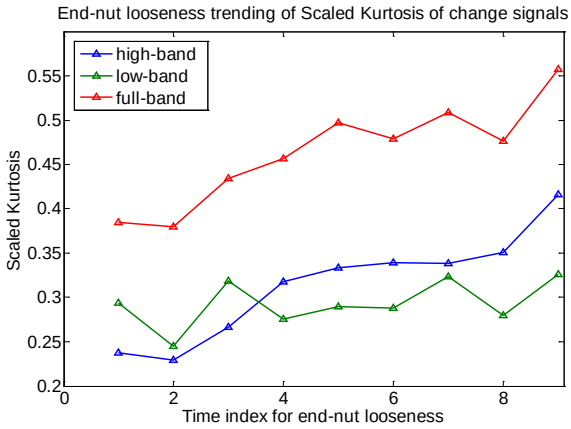

Figure 18. Trending of scaled kurtosis CI from carrier SSA (at Ring-Front sensor & cruise power) change signal with cross-over at 750th shaft order

5.3.2. Planet Carrier Plate Cracking

The helicopter main gearbox planet carrier plate cracking was not a widely known fault type until 2002 when it occurred in the UH-60A Blackhawks of US Army. Since 2004, it has also occurred in the SH-60B Seahawks of US Navy. The test data used for this paper were acquired at US Navy's HTTF in Patuxent River, Maryland.

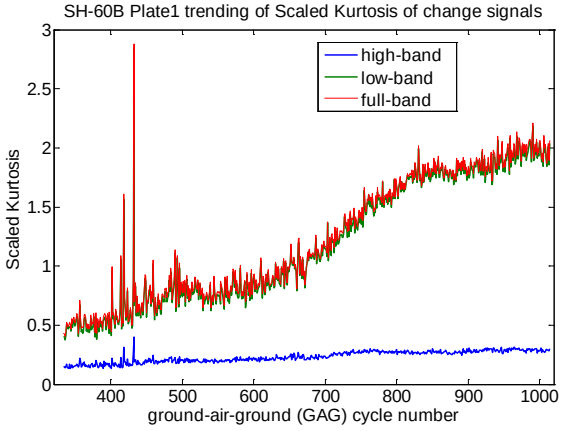

Figure 19. Trending of scaled kurtosis CI of 40% torque and STBDRING sensor at cross-over of 1700 shaft order.

Using the unified approach, we produced CIs for all the sensor data. Some results with selected HUMS sensors at 40 percent torque for the main rotor are shown in Figure 19 to Figure 21. With a cross-over frequency of 1700 orders of the carrier shaft, and vibration data from the sensor on the starboard side of the ring gear (STBDRING), the scaled kurtosis CIs versus ground-air-ground (GAG) cycle number (equivalent to a time index) are shown in Figure 19. We can see that the full (red) and low (green) band CIs track well with the changes caused by the crack propagation in which the crack lengths were known to have grown from 90mm (3.54") at GAG #410 to 172mm (6.78") at GAG #763.

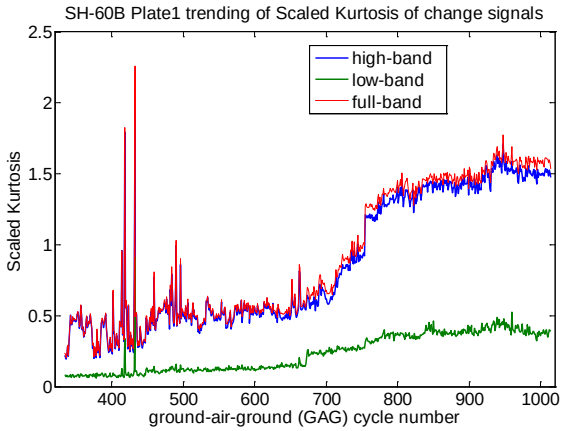

Figure 20. Trending of scaled kurtosis CI of 40% torque and VMEP1 sensor at cross-over of 500 shaft order.

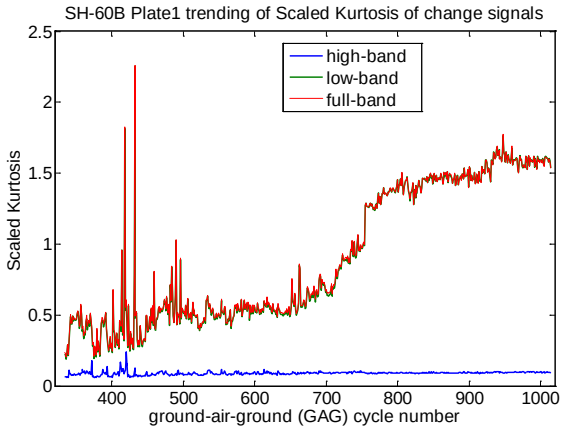

Figure 21. Trending of scaled kurtosis CI of 40% torque and VMEP1 sensor at cross-over of 1700 shaft order.

Figure 20 and Figure 21 show the results for another sensor (VMEP1, which was very close to the STBDRING sensor) at 40% main rotor torque with two different cross-over orders, i.e. 500 and 1700 orders, respectively, to show the effect of cross-over frequency on the fault detectability of the unified approach. Note that the ring gear has 228 teeth so 500 shaft orders is above the 2nd gear meshing harmonic, and there were no significant meshing harmonics beyond 1700 shaft orders. Obviously, the full band (red) CIs are identical in the two plots, which track well with the crack growth. In particular, the CI had a sudden jump at GAG #755 where the crack propagated through the outer edge of the carrier plate, which was not evident in Figure 19. Interestingly, the high band CI (blue) in Figure 20 and the low band CI (green) in Figure 21 are almost identical to the full band CIs. This means that the energy in the change signals is concentrated between 500 and 1700 orders of the carrier shaft.

Based on the results in Figure 20 and Figure 21, we can say that the selection of cross-over frequency (or order) doesn't affect fault detectability of the unified approach as a whole; it can however provide further diagnostic information on where the energy in the change signal is located in the frequency domain. The energy bandwidth in the change signals may well be utilized to distinguish the localized faults (with high bandwidth features) from the distributed faults (with low bandwidth features). We need to notice that, in this example, the cross-over orders of 500 and 1700 correspond to the frequencies of 2150Hz and 7310Hz, i.e. the order times the main rotor speed of 4.3Hz.

6. DISCUSSION AND CONCLUSIONS

In this paper we have presented a unified change detection approach to generalized health monitoring for rotating machinery. The approach is based on aligning the signals through shifting the phase spectrum of the healthy-state or reference signal by the difference in phase spectra from the future-state signal (or the signal under monitoring). The change signals are obtained from direct subtraction of the aligned signals. Condition indicators extracted from the change signals are used to detect changes caused by machine faults. Results have shown that the proposed unified approach is very effective and robust in detecting changes caused by various types of mechanical faults.

In practice, failure modes sometimes occur which were not anticipated in the development of a machine condition monitoring system, and these can often remain undetected, with potentially catastrophic consequences. It is unfortunate that we are unable to detect such faults as they happen and must come up with new techniques to detect them when they occur again. It has been our intention to develop a powerful unified fault detection method to deal with new or unexpected failure modes (or types of faults) in rotating machines. The proposed method has provided some hope in achieving that goal.

Threshold setting for the CIs is a very important aspect in HUMS and PHM systems. The kurtosis can have a threshold of 3.5 for reasons mentioned in Sections 2.1 and 4.1. The energy ratio should certainly have a threshold below 1 based on its definition in Eq. (13); hence a reasonable one would be 0.5 – meaning that the energy in

the change signal has reached 50 percent of that in the reference signal. However, there is no common threshold of scaled kurtosis for different fault types as observed in the results of this paper. From the definition of the scaled kurtosis in Eq. (14), we may look at setting the threshold upper bound to around 1, e.g. an energy ratio of 0.33 and a kurtosis of 3 ($0.33\times3\approx1$). Another way of thresholding the scaled kurtosis may be to put a limit on its rate of change (or differential). This will be an area for further study.

The other area worth further investigation is the systematic approach to selecting the reference signal. Is it always sufficient to just use the data at the beginning of the machine operation, or is it better to choose the data at the start of each run or use a moving reference signal? These are questions to be answered after further testing and validating of the proposed unified approach against a wide range of fault types.

In conclusion, we have shown that the proposed unified change detection approach is effective and robust in detecting changes caused many types of mechanical faults. It has the potential to cope with a much wider range of failure modes in rotating machinery than the existing methods. The new method is also simple in concept and fast in calculation (it only needs the FFT), and would be straightforward to implement in existing PHM systems. We anticipate that the method could be widely tested and matured in the near future.

ACKNOWLEDGEMENT

The authors would like to acknowledge Dr. David Blunt of DSTO for his review of the paper. We also give acknowledgements to JSF Program Office, US Navy, Pratt & Whitney, Rolls-Royce Corporation and Eurocopter for their collaborations.

REFERENCES

Becker, A., Peters, W. and Konzen, M. (2007). Advanced Vibration Monitoring of Sea King Input Shaft Assembly. *International Conference of Maintenance Societies*, May 2007, Melbourne, Australia.

Blunt, D.M and Keller, J.A. (2006). Detection of a fatigue crack in a UH-60A planet gear carrier using vibration analysis. *Journal of Mechanical Systems and Signal Processing 20*(8), pages 2095-2111.

Bonnardot, F., Badaoui, M.El, Randall, R.B., Daniere, J., and Guillet, F. (2005). Use of the acceleration signal of a gearbox in order to perform angular resampling (with limited speed fluctuation). *Journal of Mechanical Systems and Signal Processing 19*(6), pages 766-785.

Braun, S. (1975). Extraction of Periodic Waveforms by Time Domain Averaging. *Acoustica* 32, pages 69-77, 1975.

Burchill, R.F., Frarey, J.L. and Wilson, D.S. (1973). New machinery health diagnostic techniques using high-frequency vibration. *SAE Paper 730930*, 1973.

Forrester, B.D. (1996). *Advanced Vibration Analysis Techniques for Fault Detection and Diagnosis in Geared Transmission Systems*. Ph.D. Thesis, Swinburne University of Technology, Australia.

Galati, F.A., Forrester, B.D. and Dey, S. (2008). Application of the generalised likelihood ratio algorithm to the detection of a bearing fault in a helicopter transmission. *Australian Journal of Mechanical Engineering* 5(2), pages 169-176, 2008.

Galati, F.A. (2007). Investigation into Input Drive-Shaft Assembly Failures in RAN Sea King's. *Vertiflite Conference (AIAC12)*, 13-17 March 2007, Melbourne, Australia.

Hancock, K.M. and Zhang, Q. (2006). A Hybrid Approach to Hydraulic Vane Pump Condition Monitoring and Fault Detection. *Transaction of the American Society of Agricultural and Biological Engineers (ASABE)* 49(4): 1203−1211, 2006.

Larder, B.D. (1999). Helicopter HUM/FDR: Benefits and Developments. *Proceedings of the 55th Annual Forum of the American Helicopter Society (AHS)*, 25-27 May 1999, Montreal, Canada.

Jarvis, M.P. and Sleight, P. (2011). *Report on the Accident to Aerospatiale (Eurocopter) AS332 L2 Super Puma Registration G-REDL*. Aircraft Accident Report 2/ 2011, Air Accidents Investigation Branch, Department of Transport, UK.

Lee, E. (2010). A simple HUMS approach to detect characteristic variation for mechanical systems. *Prognostics and Health Management Conference* (PHM '10, p1-8), 12-14 Jan 2010, Macau, China.

Lei, Y.G., Lin, J., He, Z.J., and Zuo, M.J. (2013). A review on empirical mode decomposition in fault diagnosis of rotating machinery. *Journal of Mechanical Systems and Signal Processing* 35, pp. 108-126, 2013.

Man, Z.H., Wang, W., Khoo, S.Y., and Yin, J.L. (2012). Optimal Sinusoidal Modelling of Gear Mesh Vibration Signals for Gear Diagnosis and Prognosis. *Journal of Mechanical Systems and Signal Processing* 33(11), pp. 256-274, Nov. 2012.

Mcfadden, P.D. and Toozhy, M.M. (2000). Application of Synchronous Averaging to Vibration Monitoring of Rolling Element Bearings. *Journal of Mechanical Systems and Signal Processing* 14(6), pp. 891-906, June 2000.

Randall, R.B. and Antoni, J. (2011). Rolling element bearing diagnostics – A Tutorial. *Journal of Mechanical Systems and Signal Processing* 25, pp. 485-520, 2011.

Stewart, R.M. (1977). Some useful data analysis techniques for gearbox diagnostics. *Technical report paper MHM/R/10/77*, University of Southampton, Institute of Sound and Vibration Research, 1977.

Vavlitis, C. (1998). Crack Growth Behaviour of Spur Gears: A Fractographic Analysis. *DSTO-TN-0137*, Defence Science and Technology Organisation, Jan 1998, Australia.

Vecer, P., Kreidl, M. and Smid, R. (2005). Condition Indicators for Gearbox Condition Monitoring Systems. *Acta Polytechnica Report* Vol. 45, No. 6/2005, Czech Technical University Publishing House, Prague, Czech Republic.

Wang, W.Y. and Harrap, M.J. (1996). Condition Monitoring of Ball Bearings Using Envelope Autocorrelation Technique. *The International Journal of Machine Vibration* (5), pages 34-44, 1996.

Wang, W. and Wong, A.K. (2000). Linear Prediction and Gear Fault Diagnosis. *Proceedings of the 13th International Conference of Condition Monitoring and Diagnostic Engineering Management (COMADEM)* 2000, pages 305-315, December 3-8, 2000, Houston, Texas, USA.

Wang, W. (2001). Early Detection of Gear Tooth Cracking Using the Resonance Demodulation Technique. *Mechanical System and Signal processing* 15(5), pages 887-903.

Wang, W. and Keller, J.A. (2007). A Novel Technique of Crack Detection for Helicopter Main Gearbox Planet Carrier. *Proceedings of the 5th DSTO International Conference on Health and Usage Monitoring* (HUMS 2007), 13-17 March 2007, Melbourne, Australia.

Wang, W. (2008). Autoregressive Model-Based Diagnostics for Gears and Bearings. *Insight – Non-Destructive Testing and Condition Monitoring* 50(8), pages 414-418, August 2008.

Wang, W. and Muschlitz, G. (2010). Disk Crack Detection in Spin Testing Using Tip Timing Data. *31st IEEE Aerospace Conference*, March 6-13 2010, Big Sky, Montana, USA.

BIOGRAPHIES

Wenyi Wang received his PhD in Mechanical Engineering from the University of New South Wales (UNSW) and became a Lecturer at Monash University in 1996. He joined DSTO in 1998 and has been a Senior Scientist in machine dynamics and diagnostics since 2002. Wenyi has over 60 publications and has received some prestigious awards including a Defence Science Fellowship in 2007 and a Victoria Fellowship in 2001. He is currently leading a JSF Program Office funded project on advanced vibration-based PHM for JSF propulsion systems.

B. David Forrester received his PhD in Mechanical Engineering from Swinburne University of Technology in 1996. He joined DSTO in 1981, and has been doing research in machine condition monitoring and diagnostics since 1988. He has been Principal Scientist and Head of machine dynamics and diagnostics at DSTO since 2010.

Peter Frith received his PhD in Mechanical Engineering from the University of New South Wales in 1984. He joined DSTO in 1983 and his research has focused on the development of health management technologies for propulsion and power systems of military aircraft. Peter was posted to the JSF Program Office from 2003 to 2006, and he was Scientific Adviser to the Royal Australian Air Force from 2008 to 2011. He is currently the Research Leader of the Aircraft Health and Sustainment Branch in the Aerospace Division of DSTO.